Image Cover Sheet

CLASSIFICATION	SYSTEM NUMBER
UNCLASSIFIED	511144

TITLE

Gigaelectron-Volt Heavy ion Irradiation of Gallium Arsenide

System Number:

Patron Number:

Requester:

Notes:

DSIS Use only:

Deliver to:

Gigaelectron-volt heavy ion irradiation of gallium arsenide

Cosmo Carlone and Martin Parenteau
Département de Physique, Université de Sherbrooke, Sherbrooke, Québec, J1K 2R1, Canada

Shyam M. Khanna
Defence Research Establishment Ottawa, Department of National Defence, Ottawa, Ontario, K1A 0Z4, Canada

(Received 7 May 1997; accepted for publication 5 February 1998)

Gallium arsenide grown by metalorganic chemical vapor deposition and n doped with silicon to nominal concentrations of 2×10^{15}, 8×10^{15}, and 2×10^{16} cm^{-3}, was irradiated with 1.04 GeV bromine ions at a fluence of 5×10^{9} cm^{-2}, 1.7 GeV iodine ions at a fluence of 2.7×10^{9} cm^{-2}, and 1.5 GeV gold ions in the fluence range of 1.0×10^{6}–2.2×10^{9} cm^{-2}. The effects were analyzed by photoluminescence (PL) spectroscopy. The donor-to-gallium vacancy (D-V_{Ga}) and the donor-to-silicon-acceptor (D-Si_{As}) transitions are observed in the PL spectra of the irradiated samples. The former occurs at 1.476 eV, and the latter at 1.483 eV when the recording temperature is 6.5 K. The relative introduction rates of the V_{Ga} and Si_{As} defects for these ions are compared to those obtained in previous studies where electrons, protons, alpha particles, lithium ions, and oxygen ions were the irradiating particles. The measured values correlate with relativistic (Darwin–Rutherford) or nonrelativistic (Rutherford) scattering theory, depending on the projectile energy. The relevance of the GeV heavy ion irradiation with cosmic rays is discussed. © *1998 American Institute of Physics.* [S0021-8979(98)02210-5]

I. INTRODUCTION

Depending on particle type, energy, and fluence, irradiation changes the properties of matter in various ways. In the case of cosmic rays, which consist of nuclei of all the elements, their flux decreases in a nonsimple manner with the nuclear charge Z,[1] and their energy can reach 10^{20} MeV.[2] They penetrate matter and cause ionization damage to electronic circuits on space satellites. To imitate their effect, 320 MeV iodine ion irradiation was used and experiments showed that the threshold fluence for burnout phenomena in gallium arsenide (GaAs) technology is 10^{5} cm^{-2}; however, no mechanism was given.[3] Energetic particles also cause displacement damage. Using oxygen, krypton, argon, and xenon ions at energies of 0.2, 0.4, 1.4, and 5.5 GeV, respectively, the resistance of silicon-doped n-GaAs was observed to increase irreversibly.[4] The effect was attributed to the introduction of deep levels even though they were not observed. In the same work, n- and p-GaAs samples grown by the liquid encapsulated Czochralski (LEC) method and irradiated with 0.3 GeV calcium ions and 0.7 GeV zinc ions were characterized by photoluminescence (PL), but no radiation-induced defect was reported. It was observed, however, that the PL intensity of p-type GaAs decreased faster than that of n-type, but the defect creation mechanism could not be determined.

The primary motivation of the present work is to determine by PL the permanent damage caused by GeV particles incident on n-GaAs samples. In the irradiated samples studied here, the gallium vacancy (V_{Ga}) and its related defect silicon at the arsenic site (Si_{As}) were observed, providing direct evidence of displacement damage in GaAs. The observation of these specific defects suggests mechanisms which may explain some of the results found in previous investigations.[4]

Vacancy defects in irradiated GaAs have been reported. The E1 level was observed in the deep level transient spectroscopy (DLTS) data of GaAs irradiated with 1.5 MeV electrons. Its energy was determined to be 45 meV below the conduction band and the defect was attributed to the arsenic vacancy (V_{As}).[5] E1 has been observed in the DLTS spectrum of GaAs irradiated with ^{60}Co gamma rays,[6] 0.3–4 MeV electrons,[7] beta rays,[8,9] fission and reactor neutrons,[9] 2 MeV protons,[10] and 5.4 MeV alpha particles.[10,11] The PL transition at 1.4745 eV observed in the spectrum of GaAs irradiated with fission neutrons at a fluence of 10^{13} cm^{-2} was attributed to the gallium vacancy (V_{Ga}) defect.[12] The same PL transition has also been observed in GaAs irradiated with ^{60}Co gamma, 7 MeV electrons, reactor neutrons, 0.6–200 MeV protons, alpha particles, lithium, and oxygen ions.[13] The 47 cm^{-1} transition observed in the Raman spectrum of GaAs irradiated with 45 keV Be ions to a fluence of 5×10^{14} cm^{-2} was attributed to phonons associated with V_{Ga}.[14] Vacancies have not been reported in GeV heavy ion irradiated GaAs.

Besides the transition at 1.4745 eV, another transition at 1.483 eV was observed in the PL spectrum of irradiated Si-doped n-GaAs samples.[13] The transition was attributed to the Si_{As} acceptor defect. Its introduction rate has been found to increase with the doping concentration, confirming that it results from a transfer of the Si atom from the Ga site to the As site. In most samples studied previously, both the V_{Ga} and the Si_{As} appear after irradiation and annealing but their relative intensity depends on the doping concentration.

Vacancies are often invoked to explain radiation effects, even though they are not reported. For example, in the modi-

fication of quantum well band structures through irradiation followed by rapid thermal annealing, the changes were attributed to the introduction of vacancies and interstitials[15,16] but no radiation-induced defects were observed in the PL spectrum. The direct observation of the vacancies could have confirmed the details of the proposed mechanisms. The description of more complex changes, such as the phase transformations induced by low energy ion implantation,[17,18] tend to be less complete. Vacancies may play a role, and, if observed, would give a physical insight into these, and other phenomena.

II. THEORETICAL MODELS

The concentration of defects created in the primary knock out process is given by scattering theory and is proportional to the number N of atoms per unit volume of the crystal and to the fluence of the beam ϕ. For the vacancy defect V, its concentration is given by

$$[V]=N\sigma\phi, \tag{1}$$

where the proportionality constant σ is the total scattering cross section. The product $N\sigma$ is called the introduction rate and is symbolized by b.

$$b=N\sigma. \tag{2}$$

Electrons and protons above 100 MeV are relativistic. In this case, σ is calculated using the Darwin–Rutherford scattering theory, given by[19]

$$\sigma_r=\pi\left[\frac{Z_1Z_2e^2\gamma_1}{m_1c^2(\gamma_1^2-1)}\right]^2\left(\frac{E_m}{E_d}-1\right), \tag{3}$$

which is valid when the mass of the projectile is much smaller than that of the target atoms ($m_1 \ll m_2$). Z is the charge, the subscript 1 refers to the projectile, and 2 to the target atoms, E_m is the maximum energy transferred during the collision, E_d is the displacement threshold (about 9.8 eV for GaAs[10]), and

$$\gamma_1=\frac{E_1}{m_1c^2}+1,$$

where E_1 is the kinetic energy of the projectile. E_m is given by[20]

$$E_m=\frac{2m_2E_1(2m_1c^2+E_1)}{(m_1+m_2)^2c^2+2m_2E_1}.$$

Expression (3) cannot be used for heavier particles because the condition $m_1 \ll m_2$ is not satisfied. In this case, the nonrelativistic expression (Rutherford scattering) was used[19]

$$\sigma_{nr}=\pi\left[\frac{Z_1Z_2e^2(m_1+m_2)}{2m_2E_1}\right]^2\left(\frac{E_m}{E_d}-1\right), \tag{4}$$

where

$$E_m=4E_1\frac{m_1m_2}{(m_1+m_2)^2}.$$

The expression (4) is valid for projectiles of any mass. Usually, $E_m \gg E_d$ and σ varies as E_1^{-1} in the nonrelativistic case. Eqs. (3) and (4) are equivalent at low energy but, at higher energy, the relativistic effects cause a deviation from the E_1^{-1} dependence, and expressions (3) and (4) give different values.

TABLE I. Characteristics of the wafers used in the present study.

Wafer	Dopant	Doping level (cm^{-3})	Thickness (μm)
a	Si(n)	8.5×10^{15}	4.0
b	Si(n)	1.1×10^{16}	3.8
c	Si(n)	1.8×10^{16}	3.5

III. EXPERIMENT

The GaAs samples were cut from several wafers supplied by Epitronics Corporation. The wafers were grown by metalorganic chemical vapor deposition (MOCVD) on semi-insulating substrates and were intentionally n doped to nominal values of 2×10^{15} Si atoms/cm^3, 8×10^{15} Si atoms/cm^3 and 2×10^{16} Si atoms/cm^3. The wafers were 3 in. in diameter, and then cut into samples about 10 mm long and 5 mm wide. The thickness of the layers and the actual doping levels are given in Table I.

The irradiations with the heavy ions (1.04 GeV Br, 1.7 GeV I, 1.5 GeV Au) have been performed at the Atomic Energy Commission Laboratory (AECL), at Chalk River, Ontario, Canada. After irradiation, each sample was cut into two pieces, one of which was annealed at 550 °C for 30 min before returning slowly to room temperature at a rate of 50 °C/h.

The PL spectra were recorded at $T=6.5$ K. Several samples were placed in the cryostat at the same time, allowing for the samples irradiated with several fluences of a given particle to be measured in the same run. An unirradiated sample was also mounted in the cryostat and was used as a reference. The entire mount could be translated in the x, y, or z directions in order to record the PL spectrum of the samples, but the optical components were not varied. The excitation was provided by a Ti:sapphire laser tuned at 1.58 eV, with a power density of about 10 mW/cm^2. The luminescent signal was analyzed with a single monochromator and measured with a standard photomultiplier and photon counting system.

Although the penetrating depth of the probing laser light is about 0.6 μm for $\lambda=780$ nm, it was observed that the PL intensity increases linearly with the thickness of the films, up to about 10 μm, before flattening off at higher thickness.[21] This observation suggests that one investigates the defects created well beyond the penetration depth of the laser light, up to 10 μm in the present experiments. Since the sample epilayer was at most 4 μm thick, the PL experiments reported here sample most of the deposited film

IV. RESULTS AND ANALYSIS

The near band PL spectrum recorded at 6.5 K of an unirradiated n-type sample is shown in Fig. 1. It consists of excitonic transitions between 1.512 and 1.517 eV, and donor-to-acceptor transitions (D-A) between 1.46 and 1.50

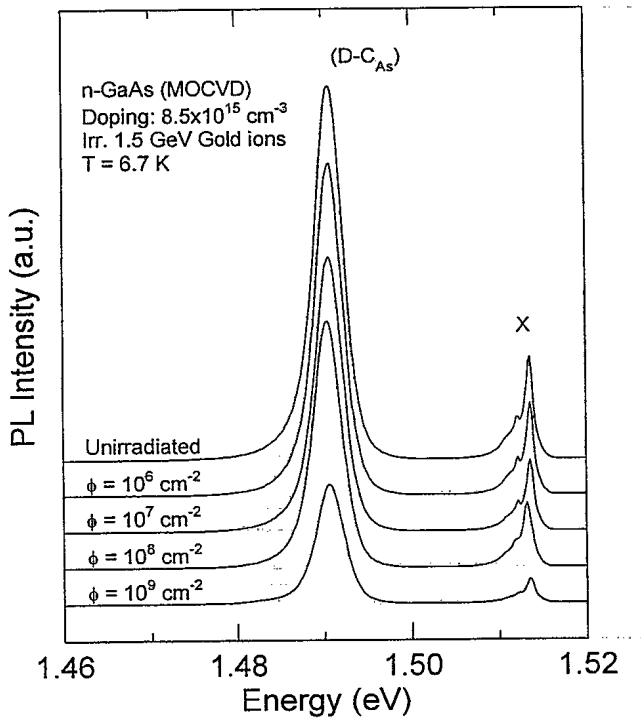

FIG. 1. The PL spectrum of n-type GaAs as a function of 1.5 GeV Au ion fluence ϕ. The samples were not annealed after irradiation. The intensity scale is the same for all five spectra but has been shifted for clarity. The excitonic transitions (X) occur at about 1.513 eV, and the donor to carbon acceptor transition (D-C_{As}) at 1.490 eV.

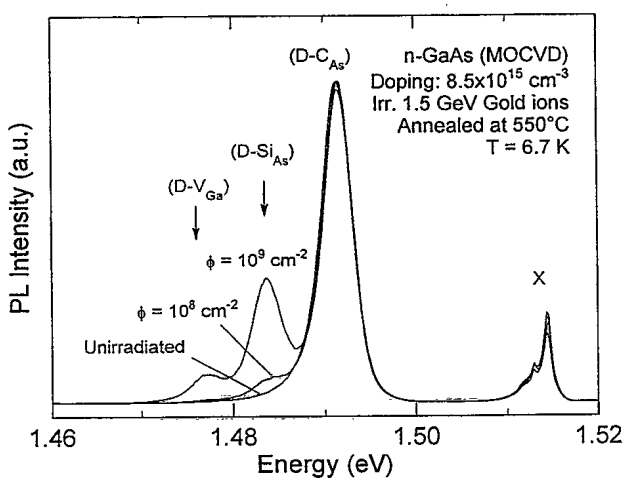

FIG. 2. The PL spectrum of n-type GaAs as a function of 1.5 GeV Au ion fluence ϕ, followed by annealing to 550 °C for 30 min. The two radiation-induced peaks are attributed to (D-V_{Ga}) and to (D-Si_{As}). These two peaks do not appear in the samples which were annealed to 550 °C for 30 min but not irradiated.

eV. The strongest feature of the excitonic transitions is attributed to an exciton recombination at a donor site. The donor is most likely silicon at the gallium site, i.e., Si_{Ga}. Carbon is a residual impurity of the growth technique and the (D-C_{As}) transition is always dominant in the PL spectrum recorded at low temperature. One effect of irradiation is to reduce the intensity of the spectrum. This is also shown in Fig. 1 for 1.5 GeV Au ion irradiation.

The reduction of the intensity has been attributed to the formation of radiation-induced complexes, which capture conduction band electrons and therefore reduce the number of transitions to the defects present prior to irradiation.[22] Annealing serves to dissociate these complexes. It was found that complexes involving the vacancies are dissociated at about 450 °C.[12] The PL signature of the V_{Ga} and Si_{As} defects is much stronger after annealing, allowing for a better estimate of their relative introduction rate. However, some of the V_{Ga} and Si_{As} defects may also recombine with other defects present in the crystal during the annealing. For example, a Ga interstitial may recombine at a V_{Ga} defect. In view of the increase of the PL intensity associated with the V_{Ga} and Si_{As} defects after annealing, these processes do not seem to dominate. Moreover, if a fraction of these two defects actually recombines during the annealing, our evaluation of the relative introduction rates should still hold, as long as the fraction of recombined defects stays approximately constant for various irradiation conditions. These recombination phenomena constitute another source of uncertainty on the relative defect introduction rates.

The radiation-induced transitions in the annealed samples are shown in Fig. 2 for 1.5 GeV Au ion irradiation. Annealing to 550 °C for 30 min restores 90% of the PL intensity, suggesting that annealing dissociates most of the radiation-induced complexes. However, the irradiation and the annealing of silicon-doped n-GaAs introduce a peak at 1.4745 eV identified as the (D-V_{Ga}) transition, and another one at 1.483 eV identified as the (D-Si_{As}) transition.[12,13] The appearance of the (D-Si_{As}) transition was explained by the reaction

$$V_{As}^{+}+Si_{Ga}^{+}+2e^{-}\rightarrow V_{Ga}^{-}+Si_{As}^{-}+2h^{+}, \tag{5}$$

where e stands for an electron and h for a hole.[23] Either (D-V_{Ga}) or (D-Si_{As}) can be used to determine a relative defect introduction rate, b.

Figure 3 shows the drop in intensity of the unannealed irradiated samples. The error bar is due to variations of the samples across the same wafer and to the reproducibility of optical conditions in analyzing different samples. At low fluences, the PL intensity is constant, and it is reduced at high fluences. The fit was based on the equation

$$\frac{1}{I}=\frac{1}{I_0}+K\phi, \tag{6}$$

where I_0 is the pre-irradiated value of the intensity and K is a degradation constant.

The intensity of the radiation-induced transitions is sensitive to the doping. In the samples doped nominally to 2×10^{15} cm^{-3}, (D-V_{Ga}) is generally weak compared to the (D-C_{As}), but it is stronger than the (D-Si_{As}) transition. In the samples doped to 2×10^{16} cm^{-3}, the opposite is true: (D-Si_{As}) is stronger than (D-V_{Ga}) and can be comparable in intensity with the (D-C_{As}) transition. Despite this doping dependence, the introduction rate of the (D-V_{Ga}) transition in the lower doped samples and the introduction rate of both transitions in the higher doped samples have been reported.[13]

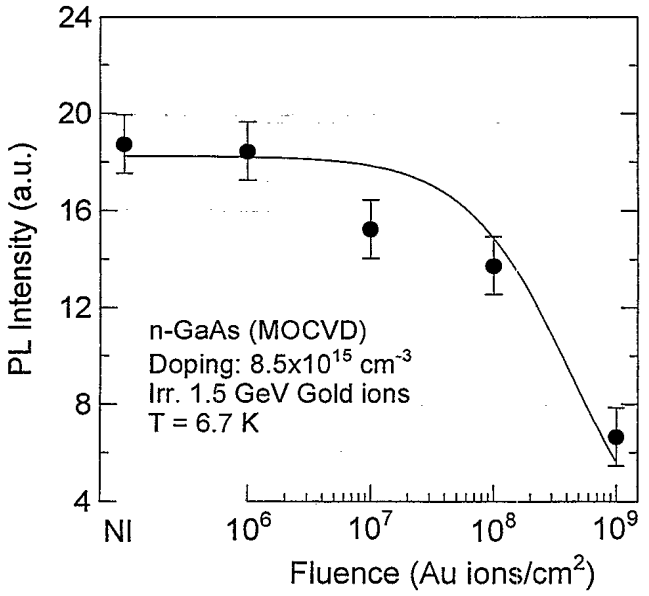

FIG. 3. A plot of $I(\text{D-C}_{\text{As}})$ as a function of fluence for 1.5 GeV Au ions, for which the samples were not annealed. The solid line is the best fit using Eq. (6).

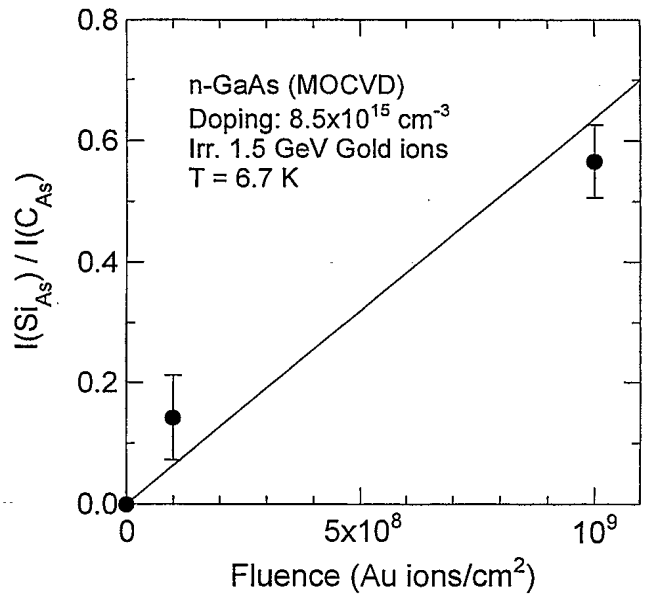

FIG. 4. A plot of $I(\text{D-C}_{\text{As}})/I(\text{D-C}_{\text{As}})$ as a function of fluence for 1.5 GeV Au ions, for annealed samples. The slope gives the relative introduction rate b.

In Ref. 13, the heaviest ion was oxygen and its energy was 30 MeV. Whenever both V_{Ga} and Si_{As} appeared in the PL spectrum, we observed that the relative introduction rate was independent of defect chosen. In other words, the two scale in the same way.

For the purpose of measuring b, maximum precision is obtained when samples doped to 2×10^{16} cm^{-3} are annealed, and when the $(\text{D-Si}_{\text{As}})$ signal is measured.[13] In order to analyze the variation of Si_{As} concentration, the ratio of the intensity of the $(\text{D-Si}_{\text{As}})$ peak over the intensity of the (D-C_{As}) peak was taken. Assuming that the carbon concentration is not affected by irradiation, any variation of the PL intensity due to changes in the optical alignment or to the creation of deeper levels is eliminated.

Figure 4 shows the increase of the $(\text{D-Si}_{\text{As}})$ intensity, normalized to the (D-C_{As}) intensity, in the annealed samples, as a function of fluence. The slope is proportional to the introduction rate b. Although the signal associated with $(\text{D-Si}_{\text{As}})$ in Fig. 2 at 10^8 cm^{-2} is roughly one tenth that at 10^9 cm^{-2}, indicating a linear introduction rate at these fluences, for some of the other particles, the fluences were so high that the $(\text{D-Si}_{\text{As}})$ transition could be as much as 30 times that of (D-C_{As}), and a saturation of the ratio $I(\text{D-Si}_{\text{As}})/I(\text{D-C}_{\text{As}})$ was observed. For these cases, that ratio was plotted as a function of the irradiation fluence, and the curve obtained was modeled with an inverse tangent function[13]

$$\frac{I(\text{D-Si}_{\text{As}})}{I(\text{D-C}_{\text{As}})} \propto \frac{2S}{\pi} \arctan\left(\frac{b\pi}{2S}\,\phi\right). \tag{7}$$

The inverse tangent shape was chosen to account for the saturation observed in the experimental data at high fluences and for the linear dependence at low fluence. The parameter b, which is the slope at low fluence, is the introduction rate, and S is the value of the ratio when saturation is reached. All the introduction rates were arbitrarily multiplied by 0.5×10^{15} in order to get values closer to unity. The S value was about ten times higher in the samples doped to 2×10^{16} cm^{-3}, compared to those doped to 2×10^{15} cm^{-3}, confirming reaction (5).

The PL spectra of GaAs irradiated with various particles are shown in Fig. 5. The fluences shown give about the same intensity for the $(\text{D-Si}_{\text{As}})$ transition, but the intensity of the (D-V_{Ga}) transition is not constant. It is not observed in the spectrum of proton, alpha, and lithium ion irradiated GaAs at the fluence shown, but is observed at higher fluences. The spectra are available in Ref. 13. Although a correction could in principle be made to account for the different doping levels of the wafers a, b, and c, that correction is not easy to evaluate. Since the doping levels of our samples are rather similar, it was decided to consider the raw PL spectra. This variation in doping concentration constitutes the major source of error in calculating the introduction rates.

Figure 6 presents the b values for the heavy ions studied here, as well as other particles studied previously. The dashed lines are based on relativistic theory, the solid ones on nonrelativistic theory.

V. DISCUSSION OF THE INTRODUCTION RATES

It is seen from Fig. 6 that the measured relative introduction rates, from electrons to Au ions, tend to agree with the scattering cross sections for the various particles, as calculated with Eqs. (3) and (4). The data for light particle irradiations are modeled with the relativistic Darwin–Rutherford expression (3) while the data for heavy ion irradiation are modeled with the nonrelativistic Rutherford expression (4). In the cross section calculations, we used the atomic number of the irradiating particles as their charge Z_1, assuming that they are totally stripped from all their electrons when they interact with the ions of the GaAs crystal.

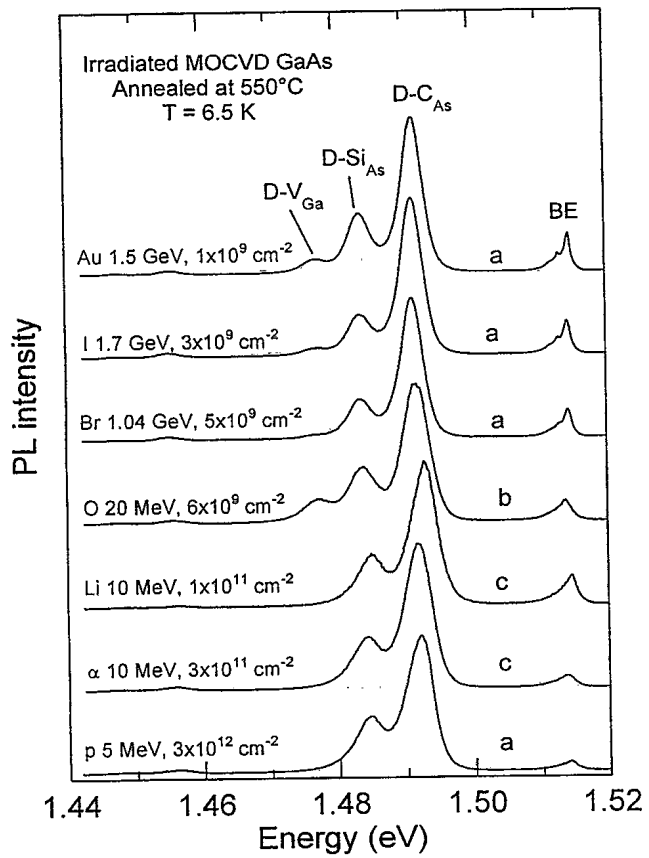

FIG. 5. PL spectra at $T = 6.5$ K for samples irradiated with the heavy ions used in this study. The spectra shown have been chosen with fluences that give similar concentrations of Si_{As} defects. For lighter irradiating particles, higher fluences are necessary to produce an equivalent concentration of Si_{As} defects. The letter a, b, or c above each curve indicates the corresponding wafer (see Table I).

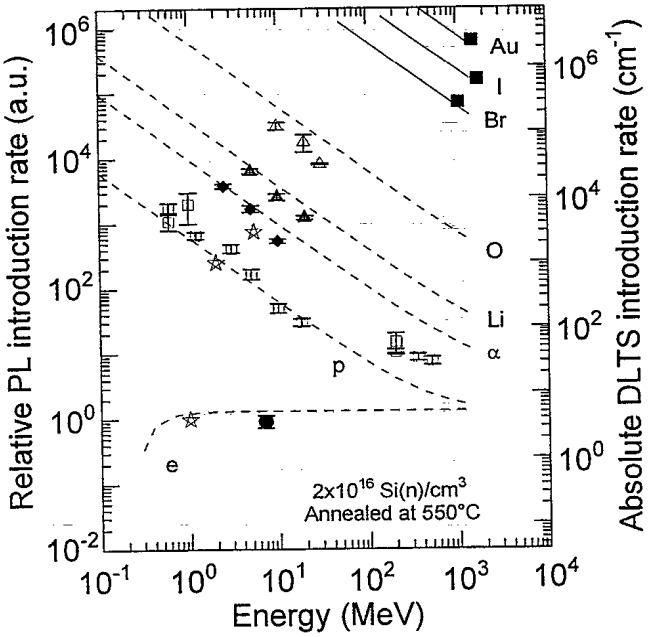

FIG. 6. Introduction rate of the Si_{As} defect as a function of the energy of various irradiating particles. The Darwin–Rutherford formula (3) was used for irradiations with electrons and light ions (dashed curves), and the Rutherford formula (4) for the heavier ions (solid curves). Absolute values of the introduction rate are given by the scale at the right. For 1 MeV electron irradiation, the scale on the right gives the theoretical value of 3.98 cm^{-1}. The DLTS values, indicated by a star, are included for 2 MeV proton and 5.4 MeV α irradiations.

The good agreement between the experimental and theoretical values indicates that this assumption may be valid. If the projectiles are not totally stripped from their electrons, at least their charge is proportional to their atomic number. The good agreement between theory and experimental results is not entirely expected because V_{Ga} and Si_{As} are also created by secondary collisions and possibly by annealing. Regarding secondary collisions, the experiments reported here probe a distance which is very short compared to the stopping range of the energetic particles. Since most of the incident particles go right through this probed layer, the fluence associated with the secondary ions emitted from the layer sampled is small compared to that of the incident particles. If one were to probe a longer distance, or if one were to reduce considerably the ion energy, the role of the secondary ions would become more important. According to simulations,[24] the stopping range of 1.5 GeV gold ions is 54 μm, which is more than ten times the thickness sampled.

Regarding the annealing process, the MOCVD samples investigated in this work were grown at temperatures of about 600 °C and annealing them to the growth temperature should not introduce more defects. It was observed that annealing the unirradiated samples studied here to 550 °C did not introduce the radiation-induced peaks shown in Fig. 2. Thus we do not think that annealing to 550 °C by itself introduces vacancies. What happens after irradiation and annealing is speculative. Nevertheless, the observation of Si_{As} in the PL spectrum of the unannealed sample suggests that V_{As}, or a complex containing V_{As}, diffuses through the crystal and when it comes near the dopant atom (Si_{Ga}) then silicon switches lattice site. The experiments suggest that the V_{Ga} defect is stable up to 550 °C in the materials studied in this work. The intensity increase of the ($D\text{-}V_{Ga}$) transition due to annealing can be explained by the dissociation of radiation-induced complexes. If V_{Ga} is created in the dissociation process, it is stable. If V_{As} is created, its diffusion results in V_{Ga} only when it reaches Si_{Ga}. The complexes are not known, but the divacancy (V_{As}-V_{Ga}) and others involving interstitials are likely candidates. The agreement between experiment and scattering theory could suggest that the number of defects introduced by the secondary collisions and annealing is relatively small.

We used Si_{As} to measure the relative introduction rate of V_{Ga}. This amounts to assuming that all the Si_{As} defects are generated by the mass Eq. (5). If silicon switches lattice site through another mechanism, then the measured introduction rates based on Si_{As} could be higher than the ones calculated for V_{Ga}. Conversely, V_{Ga} could result from processes that do not involve the Si_{As}. It has been observed[13] that when both defects appear after irradiation and annealing, their introduction rates follow the same trends (as a function of the type and energy of irradiating particles). One can then choose either defect to measure the relative defect introduction rates. As mentioned in Sec. I and in Sec. IV, the ratio between the

TABLE II. Characteristics of the shallowest DLTS trap (attributed to V_{As}).

Activation energy (meV)	Capture σ (10^{-16} cm^{-2})	Introduction rate b (cm^{-1}) Exper.	Theory	Trap label	Ref.	Particle	Energy (MeV)	Material[a]
45	22	1.5	3.98	$E1$	[c]	Electron	1	Oriented LEC
45	Not given	1		$E1$	[d]	Electron	0.3–2	MOCVD
41	5	2.0		$E\beta1$	[e]	Beta	2.3	MOCVD
41	6	1.0		$En1$	[f]	Neutron	1–66	MOCVD
33	3	Not given[b]		$E1$	[g]	Gamma	1.1, 1.3	VPE
27	0.12	Not given		$E\alpha1$	[h]	He ions	0.05	MOCVD
26	0.15	2963	3001	$E\alpha1$	[i]	Alpha	5.4	MOCVD
24	0.08	2		$E\beta1$	[h]	Beta	2.3	MOCVD
23	0.09	1056	1013	$Ep1$	[i]	Proton	2.0	MOCVD

[a]All the materials grown by MOCVD had the same characteristics: they were n-type, doped with silicon to 2×10^{16} cm^{-3}. The samples used in Ref. 7 were the same as those used in this PL work.
[b]In this work, the gamma irradiation is given in rads. For a discussion of gamma and electron irradiation, see Ref. 13.
[c]Reference 5.
[d]Reference 7.
[e]Reference 8.
[f]Reference 9.
[g]Reference 6.
[h]Reference 11.
[i]Reference 10.

two introduction rates usually depends on the doping concentration and on the type of crystal growth.

Theory predicts absolute introduction rates, which are measured by non-optical techniques, usually DLTS and sometimes transport. Their results are now discussed.

VI. DATA FROM OTHER TECHNIQUES

A. The DLTS E1 level

The introduction rate for the E1 level was first measured with relativistic electrons (approximately 1 MeV),[5] and it has been measured several times using n-type samples with different doping concentrations and with p-type samples. Consistently, $b\approx1-2$ cm^{-1}. Putting numerical values into Eq. (4) ($m_2=74.9$, $Z_2=33$, and $E_d=9.8$ eV, Ref. 10) gives for 1 MeV electrons

$$b=3.98 \text{ cm}^{-1},$$

which is a little higher than the experimental value. It has been pointed out, however, that, due to the formation of complexes, one should add all the defect introduction rates, and the sum obtained should be compared to b.[25] Equations (3) and (4) suggest that the theory can also be tested by varying Z_1, the charge of the projectile. DLTS experiments where the projectile is varied have been performed. Table II lists presently available data on samples similar to those used in this optical study. The sample used in Ref. 7 was purchased from the Epitronics Corp. and comes from the same source as those used in this PL study. A label is sometimes added to level E1, in order to indicate the incident particle. There is a large variation of the measured value of the activation energy. This effect has been attributed to the field dependence of the measured change in capacitance.[26] Nevertheless, the agreement between theory and the experiment for three incident particles is very good (Table II). The absolute introduction rates for these three particles are shown in Fig. 6. The relative rates have been displaced so as to coincide with the absolute ones. The optical data do not give absolute introduction rates.

B. Data from transport

In the analysis of electron-irradiated n-type GaAs using transport theory, it was deduced that the irradiation introduces an acceptor defect at a rate of about 4 cm^{-1}.[27] The introduction rate is similar to that predicted by scattering theory. In Ref. 27, the acceptor defect was attributed with reservations to V_{As}, because V_{As} is intuitively a donor defect, and no other acceptor had been reported. It is possible that the acceptor of Ref. 27 is V_{Ga}.

Both these techniques confirm that the introduction rates are given by scattering theory. It is inferred that the corrections due to secondary collisions are not significant in experiments where the distance probed is much less than the stopping range.

VII. APPLICATIONS

For the GeV incident particles studied in this work, the signature of the Si_{As} and V_{Ga} defect appears in the spectrum of the irradiated GaAs samples, proving that these particles cause displacement damage. The effect of these defects on the electron mobility has appeared.[23] Similarly, their effect on the PL intensity has been reported.[22] To reproduce their relative introduction rate, the bare charge of the incident particle and of the target nuclei was used in the Darwin–Rutherford scattering theory. This suggests that, although the incident particles have gained energy in the acceleration and lost some electrons in the process, they are stripped of the other electrons during the collision. The Darwin–Rutherford theory was used for electron irradiation, and experiments

suggest that it should be used for proton irradiation in which the incident energy exceeds 100 MeV.[28] It is expected that the displacement damage observed for GeV particles will also be observed for cosmic rays, but the production rate would be given by relativistic scattering theory.

VIII. CONCLUSION

GeV heavy ion irradiation causes displacement damage when these particles pass through GaAs. The relative introduction rate of V_{Ga} is deduced through the observation of the Si_{As} defect. It correlates with Darwin–Rutherford scattering theory in which the nuclear charges of the incident and target atoms are used. The relativistic expression had been used previously to fit the introduction rates for light particle irradiations. In the present work, the nonrelativistic (Rutherford) approximation of the model has been applied successfully to fit the introduction rate of GeV heavy ion irradiations.

[1] J. Feynman and S. B. Gabriel, IEEE Trans. Nucl. Sci. **43**, 344 (1996).
[2] R. A. Mewaldt, in *Interplanetary Particle Environment*, edited by J. Feynman and S. B. Gabriel (Jet Propulsion Lab., Pasadena, CA, 1988), Publ. 88-28, p. 21.
[3] C. Barileau, A. Bensoussan, F. Brasseau, and P. Calvel, in *IEEE Nuclear and Space Radiation Effects Conference, Radiation Effects Data Workshop Record* (IEEE Service Center, Piscataway, NJ, 1996), p. 88.
[4] R. Carin, R. Madelon, D. Julienne, F. Crueze, and A. Hairie, Nucl. Instrum. Methods Phys. Res. B **63**, 21 (1992).
[5] D. Pons and J. C. Bourgoin, J. Phys. C **18**, 3839 (1985).
[6] S. T. Lai, D. Alexiev, and B. D. Nener, J. Appl. Phys. **78**, 3686 (1995).
[7] B. Lehmann, M. Briere, D. Beaunig, and A. L. Barry, in *Proceedings of the Electronic Components Conference*, Noordwijk, The Netherlands, 13–16 Nov. 1990 (European Space Agency, Paris, 1991), p. 287.
[8] F. D. Auret, S. A. Goodman, G. Myburg, and W. E. Meyer, Appl. Phys. A: Solids Surf. **56**, 547 (1993).
[9] F. D. Auret, A. Wilson, S. A. Goodman, G. Myburg, and W. E. Meyer, Nucl. Instrum. Methods Phys. Res. B **90**, 387 (1994).
[10] S. A. Goodman, F. D. Auret, and W. E. Meyer, Nucl. Instrum. Methods Phys. Res. B **90**, 349 (1994).
[11] F. D. Auret and S. A. Goodman, Appl. Phys. Lett. **68**, 3275 (1996).
[12] A. Jorio, A. Wang, M. Parenteau, C. Carlone, N. L. Rowell, and S. M. Khanna, Phys. Rev. B **60**, 1557 (1994).
[13] S. M. Khanna, A. Jorio, C. Carlone, M. Parenteau, A. Houdayer, and J. W. Gerdes, Jr., IEEE Trans. Nucl. Sci. **42**, 2095 (1995).
[14] T. Sauncy, M. Holz, and R. Zallen, Phys. Rev. B **50**, 10 702 (1994).
[15] H. H. Tan, J. S. Williams, C. Jagadish, P. T. Burke, and M. Gal, Appl. Phys. Lett. **68**, 2401 (1996).
[16] P. G. Piva, S. Charbonneau, I. V. Mitchell, and R. D. Goldberg, Appl. Phys. Lett. **68**, 2252 (1996).
[17] K. K. Tiong, P. M. Amirtharaj, F. H. Pollack, and D. E. Aspnes, Appl. Phys. Lett. **44**, 122 (1984).
[18] R. P. Sharma, R. Bhadra, L. E. Rehn, P. M. Baldo, and M. Grimditch, J. Appl. Phys. **66**, 152 (1989).
[19] F. Seitz and J. S. Koehler, in *Solid State Physics*, edited by F. Seitz and D. Turnbull (Academic, New York, 1956), Vol. 2, p. 307.
[20] L. D. Landau and E. M. Lifschitz, in *The Classical Theory of Fields* (Pergamon, London, 1962), Chap. 2.
[21] M. Parenteau, Wu Fengmei, A. Jorio, and C. Carlone, J. Appl. Phys. **77**, 5185 (1995).
[22] S. M. Khanna, A. Houdayer, A. Jorio, C. Carlone, M. Parenteau, and J. W. Gerdes, Jr., IEEE Trans. Nucl. Sci. **43**, 2601 (1996).
[23] A. Jorio, M. Parenteau, M. Aubin, C. Carlone, S. M. Khanna, and J. W. Gerdes, Jr., IEEE Trans. Nucl. Sci. **41**, 1937 (1994).
[24] J. F. Ziegler, J. P. Biersack, and U. Littmart, in *The Stopping and Range of Ions in Solids* (Pergamon, New York, 1985), Vol. 1.
[25] D. Pons, P. M. Mooney, and J. C. Bourgoin, J. Appl. Phys. **51**, 2038 (1980).
[26] S. A. Goodman, F. D. Auret, and W. E. Meyer, Jpn. J. Appl. Phys., Part 1 **33**, 1949 (1994).
[27] D. C. Look and J. R. Sizelove, J. Appl. Phys. **62**, 3660 (1987).
[28] C. Carlone, M. Parenteau, A. Houdayer, P. Hinrichsen, and J. Vincent, IEEE Trans. Nucl. Sci. **44**, 1856 (1997).

#511144